Letter

Evolution of topological charge through chiral anomaly transport

Zilin Yuan [1,2,*] Anping Huang [1,†] Wen-Hao Zhou [3,4,5,‡] Guo-Liang Ma,[3,4,§] and Mei Huang[1,‖]

[1]*School of Nuclear Science and Technology, University of Chinese Academy of Sciences, Beijing 100049, People's Republic of China*

[2]*Institue of High Energy Physics, Chinese Academy of Sciences, Beijing 100049, People's Republic of China*

[3]*Key Laboratory of Nuclear Physics and Ion-Beam Application (MOE), Institute of Modern Physics, Fudan University, Shanghai 200433, China*

[4]*Shanghai Research Center for Theoretical Nuclear Physics, NSFC and Fudan University, Shanghai 200438, China*

[5]*Faculty of Science, Xi'an Aeronautical Institute, Xi'an 710077, China*

(Received 5 December 2023; accepted 16 February 2024; published 18 March 2024)

Built upon the state-of-the-art model a multiphase transport, we develop a new module of chiral anomaly transport (CAT) to trace the evolution of the initial topological charge of the gauge field created through sphaleron transition at finite temperature and the external magnetic field in heavy-ion collisions. The eventual experimental signals of the chiral magnetic effect (CME) have been measured. The CAT explicitly shows the generation and evolution of the charge separation, the signals of the CME through the CAT are quantitatively in agreement with the experimental measurements in Au+Au collisions at $\sqrt{s} = 200$ GeV, and the centrality dependence of the CME fraction follows that of the fireball temperature. Our simulation supports the generation of the CME.

DOI: 10.1103/PhysRevC.109.L031903

Introduction. The matter-antimatter asymmetry or baryon number asymmetry of our universe is tightly related to the the topological θ vacuum configurations of gauge fields, and the electroweak baryongenesis through C and CP-violated sphaleron transition [1–3] is not enough to explain the measurement, which calls for new extension of the additional sources of CP violation.

The θ vacuum of the quantum chromodynamic dynamics (QCD) gauge field is characterized by the integer Chern-Simons number [4], and the tunneling transition through instanton or sphaleron across the energy barriers leads to nonconservation of the axial current

$$\partial^\mu j^5_\mu = 2\sum_f m_f \langle \bar{\psi} i\gamma_5 \psi \rangle_A - \frac{N_f g^2}{16\pi^2} F^a_{\mu\nu} \tilde{F}^{\mu\nu}_a, \qquad (1)$$

thus there is a chirality imbalance between the left-handed and right-handed quarks $N_5 = N_L - N_R = \int d^4x \partial_\mu j^\mu_5$ [5–8]. It has been proposed that local P and CP-odd domains can be formed in heavy-ion collisions or early universes [9–12]. In noncentral heavy-ion collisions, the strong magnetic field with the largest strength of about 10^{14} T can be produced For the system with a net chirality imbalance characterized by μ_5 for massless quarks with charge Q_e, there is a charge current **J** produced along the direction of the magnetic field **B**, which is called the chiral magnetic effect (CME) [13]. The CME charge current induces a separation of positively and negatively charged particles perpendicular to the reaction plane. Therefore, the chiral anomaly and the CME in the early stage turn into an observable effect of charge separation in the final freeze-out state [14]. An observation of the CME would verify the fundamental property of QCD, which would provide a natural solution to the baryon number asymmetry of our universe.

The main observables of the CME is the charge azimuthal two-particle correlation:

$$\gamma = \langle \cos(\phi_\alpha + \phi_\beta - 2\Psi_{\rm RP}) \rangle, \qquad (2)$$

where ϕ_α, ϕ_β, and $\Psi_{\rm RP}$ denote the azimuthal angles of produced charged particles and the reaction plane, respectively, and α and β represent either the positive or negative charges. A positive opposite-sign (OS) correlator and a negative same-sign (SS) correlator are expected to occur for the CME. This feature of the CME has been observed by measurements of the correlator γ by the STAR Collaboration for Au+Au collisions at $\sqrt{s_{NN}} = 200$ GeV [15,16] and by the ALICE Collaboration for Pb+Pb collisions at $\sqrt{s_{NN}} = 2.76$ TeV [17].

Difficulty in detecting CME signals is due, on the one hand, to the complexity of the backgrounds, including elliptic flow [18], resonance decays [19], and local charge conservation [20,21]. Most of the sign-independent background can be

*yuanzilin20@mails.ucas.ac.cn
†huanganping@ucas.ac.cn
‡zhouwenhao@xaau.edu.cn
§glma@fudan.edu.cn
‖huangmei@ucas.ac.cn

Published by the American Physical Society under the terms of the Creative Commons Attribution 4.0 International license. Further distribution of this work must maintain attribution to the author(s) and the published article's title, journal citation, and DOI. Funded by SCOAP³.

effectively eliminated by calculating the difference between OS and SS γ:

$$\Delta\gamma = \gamma_{\rm os} - \gamma_{\rm ss}. \tag{3}$$

On the other hand, since the CME signals are mostly generated in the early stage of heavy-ion collisions, the final state interactions attenuate the initial CME signal [22]. Therefore, several hard experimental attempts have been made to detect or even extract the CME signal [23,24]. For example, recent measurements using the two-plane method [25,26] have shown that the CME signal contributes no more than 10% to the total observable [27].

From the theoretical simulation side, the CME results from UrQMD and HIJING were inconsistent with the STAR experimental measurements [28], and the anomalous-viscous fluid dynamics (AVFD) model [29–31] and the a multiphase transport (AMPT) model [22,32,33] have been developed to interpret the data. These models can well describe other physical quantities except the chiral magnetic effect due to the absence of the cooperative effect of chiral anomaly and the magnetic field. The AMPT model has an advantage to simulate parton evolution and has been widely used in heavy-ion collisions. The AVFD implements the dynamical CME transport in the realistic environment of a relativistically expanding viscous fluid and provides the quantitative link between the CME transport and the experimental signal. However, The AVFD is based on hydrodynamics and does not incorporate the signal from the nonequilibrium stage, during which the magnetic field is at its maximum. It has been summarized in Ref. [34], that theoretical uncertainties originate from the initial distribution of axial charges, the evolution of the magnetic field, the preequilibrium dynamics, the hadronic phase and freeze-out conditions. In this work, we provide a theoretical framework called chiral anomaly transport (CAT) to reduce these uncertainties. CAT adds the important chiral kinetic equation on top of the existing AMPT tool, and its hadronization process naturally respects three-dimensional momentum conservation and local charge conservation.

The CAT module. Built upon the state-of-the-art model AMPT [35], the CAT module can provide a quantitative connection between the initial topological charge and the eventual experimental signal by simulating the chiral anomalous transport in heavy-ion collisions.

The structure and flow chart of CAT is illustrated in Fig. 1. The CAT module incorporates the chiral kinetic equation to substitute the ZPC module in the AMPT model. This modification allows for the simulation of the dynamical evolution of chiral quarks in the presence of a strong magnetic field within the expanding fireball. In this model, the program begins with a specified initial condition of quark distribution and chirality imbalance. The initial quark distribution is generated by the HIJING module. Chiral quarks undergo dynamical evolution within a strong magnetic field, giving rise to a CME current. This current, in turn, results in charge separation within the quark-gluon plasma (QGP). Eventually, after undergoing the quark coalescence and hadron rescattering stages, this charge separation manifests as a dipole term within the azimuthal angle distribution of positively and negatively charged hadrons. Such a dipole signal can be measured by the difference

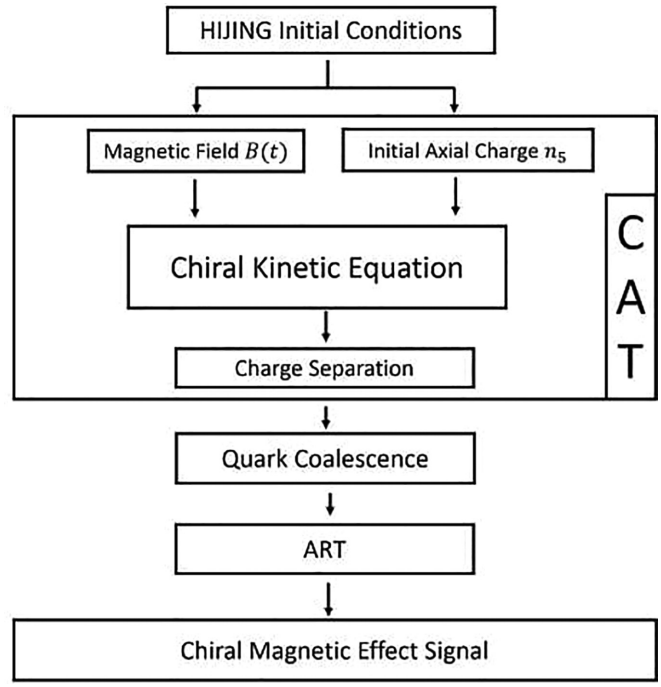


FIG. 1. Illustration of the structure of the chiral anomaly transport model based on the AMPT model. The initial nucleons and partons came from HIJING. The main part of CAT corresponds to the parton cascade, which includes the magnetic field, the axial charge, and the chiral kinetic theory. All freeze-out partons combine with hadrons and the hadron rescattering is based on the relativistic transport model (ART) model. The CME signal is calculated by the final particle.

between SS and OS charged hadron pair correlations $\Delta\gamma = \gamma_{\rm os} - \gamma_{\rm ss}$. The time required to simulate one event using one CPU core is 8–25 s, which depends on the centrality and is much slower than the original AMPT. In this paper, we generated 1.5×10^7 events for each set of parameters.

Chiral kinetic equation. The core of CAT is to solve the chiral kinetic equation, and for massless particles in the magnetic field it takes the following form [36–40]:

$$\left[\partial_t + \dot{\mathbf{x}} \cdot \boldsymbol{\nabla}_x + \dot{\mathbf{p}} \cdot \boldsymbol{\nabla}_p\right] f_i(\mathbf{x}, \mathbf{p}, t) = C[f_i], \tag{4}$$

$$\sqrt{G}\dot{\mathbf{x}} = \mathbf{v} + q_i \mathbf{B}(\mathbf{v} \cdot \mathbf{b}), \quad \sqrt{G}\dot{\mathbf{p}} = q_i \mathbf{v} \times \mathbf{B}, \tag{5}$$

where $\mathbf{x}$ and $\mathbf{p}$ represent position and momentum vectors, respectively; q_i is the quark charge; $\mathbf{b} = h\frac{\mathbf{p}}{2|\mathbf{p}|^3}$ denotes the Berry curvature, where $h = \pm 1$ represents the helicity; and $\mathbf{B}$ stands for the magnetic field. The factor $\sqrt{G} = 1 + h\frac{\hbar \mathbf{B}\cdot\mathbf{p}}{2|\mathbf{p}|^3}$. In the above, f_i represents the distribution function of a specific quark denoted by $i = (\text{flavor}, h)$, where flavor can take u, d, and s. In the CAT module, the distribution function f_i is discretized by the formula of N_i point particles (partons or quarks), i.e., $f_i(\mathbf{x}, \mathbf{p}, t) \approx \sum_{j=1}^{N_i} \delta[\mathbf{x} - \mathbf{x}_j(t)]\delta[\mathbf{p} - \mathbf{p}_j(t)]$. In the classical method, the properties of a point particle are expressed by its phase space coordinates $(\mathbf{x}_j, \mathbf{p}_j)$. However, for chiral fermions, the phase space should be extended to include the helicity or chirality parameter $(\mathbf{x}_j, \mathbf{p}_j, h_j)$. As done in the CAT module, we employ the particle simulation

method to numerically solve the kinetic equation for modeling the evolution of chiral quarks under a strong magnetic field. However, because the mass of quarks in the AMPT model is finite but small, $\mathbf{b}$ and $\sqrt{G}$ should be modified to $\mathbf{b} = h\frac{\mathbf{p}}{2\mathbf{E_p}^3}$ and $\sqrt{G} = 1 + h\frac{\hbar\mathbf{B}\cdot\mathbf{p}}{2\mathbf{E_p}^3}$ in the equation of motion and the helicity should still be treated as a good quantum number [41].

CAT solves the kinetic equation, Eq. (4), step by step from initialization. In this kinetic transport process, the charged chiral particles tend to move along the magnetic field. The direction of motion is decided by their charge and helicity. Therefore, we expect the charge separation to occur in the case of the chiral anomaly, and for the same charge, the helicity will split in space automatically. Notice that quarks and their antiquarks with the same helicity have opposite chirality and opposite charges leading to opposite splitting. The possibility of a localized chemical potential and chirality depends on the quark distribution.

Initial magnetic field and evolution of magnetic field. Following Ref [42], the initial electromagnetic (EM) field at $t_0 = 0$ fm/c is calculated from spectator protons in HIJING as follows:

$$e\mathbf{E}_0(r) = \alpha_{\rm EM}\sum_n Z_n \frac{R_n\left(1-\mathbf{v}_n^2\right)}{\left[\mathbf{R}_n^2 - (\mathbf{v}_n\times\mathbf{R}_n)^2\right]^{3/2}},$$
$$e\mathbf{B}_0(r) = \alpha_{\rm EM}\sum_n Z_n \frac{\mathbf{v}_n\times\mathbf{R}_n\left(1-\mathbf{v}_n^2\right)}{\left[\mathbf{R}_n^2 - (\mathbf{v}_n\times\mathbf{R}_n)^2\right]^{3/2}}, \quad (6)$$

where $R_n = r - r_n'$ is the relative position vector from a field point r to a source point r_n' at the initial time t_0, and $\alpha_{\rm EM}$ is the EM fine-structure constant, defined as $\alpha_{\rm EM} = e^2/4\pi \approx 1/137$. It should be noticed that the direction of the magnetic field in CAT is opposite to the y axis, due to the initial condition of target and projectile nucleons.

The evolution of the magnetic field in the parton cascade part relates to time [43,44], as follows:

$$e\mathbf{B}(t,\mathbf{x}) = \frac{e\mathbf{B}(0,\mathbf{x})}{1+\left(\frac{t}{\tau_B}\right)^2}, \quad (7)$$

where $\tau_B = 0.4$ fm/c is an effective lifetime of the magnetic field.

Chirality, helicity, and initial axial charge. It should be noted that the helicity $h = \pm$ and the chirality $\chi = R/L$ are the same for quarks but opposite for antiquarks. Their densities are denoted as follows: $n_R = n_+$, $n_L = n_-$, $\bar{n}_R = \bar{n}_-$, and $\bar{n}_L = \bar{n}_+$. The net particle density $n = \langle\bar{\psi}\gamma^0\psi\rangle = (n_R - \bar{n}_R) + (n_L - \bar{n}_L)$ could be expressed as $n = (n_+ - \bar{n}_-) + (n_- - \bar{n}_+)$, and the net chirality $n_5 = \langle\bar{\psi}\gamma^0\gamma^5\psi\rangle = (n_R - \bar{n}_R) - (n_L - \bar{n}_L) = \langle h\rangle$ could be expressed as $n_5 = (n_+ + \bar{n}_+) - (n_- + \bar{n}_-)$. For convenience, we just consider the helicity of quarks and antiquarks in the program. At the initial stage, $N_+ = (N_{\rm total} + N_5)/2$ particles are randomly selected as positive helicity, and the remaining $N_- = (N_{\rm total} - N_5)/2$ particles are assigned as negative helicity, where $N_5 = \int d^3x n_5$ represents the total chirality.

The initial local chirality density $n_5 = \mu_5^3/(3\pi^2) + (\mu_5 T^2)/3$, with T being the local effective temperature from energy density [45] and chiral chemical potential μ_5, can be either positive or negative with equal chance from event to event. μ_5 can be calculated through the sphaleron transition rate as $\mu_5 = \sqrt{3\pi}\sqrt{(320N_f^2\Gamma_{\rm ss}/T^2 - T^2/3)}$ [46]. At finite temperature and under the magnetic field, the sphaleron transition rate has the form of $\Gamma_{\rm ss}(B,T) = \frac{(g_s^2N_c)^2}{384\sqrt{3\pi^5}}(eBT^2 + 15.9T^4)$ in Ref. [47], and the chiral chemical potential can be roughly estimated as $\mu_5 \sim (aT + b\sqrt{eB})$. It should be emphasized that μ_5 can be positive or negative in local domains created event by event through heavy-ion collisions, and one can understand μ_5 in the meaning of average variance $\sqrt{\langle\mu_5^2\rangle_{\rm event}}$. Similarly, the chiral charge number N_5, in the CAT module, is equivalent to the average variance of the chiral charge number for all of the events defined in Ref. [31], specifically defined as $N_5 = \sqrt{\langle N_5^2\rangle_{\rm event}}$, which remains positive and constant for each event.

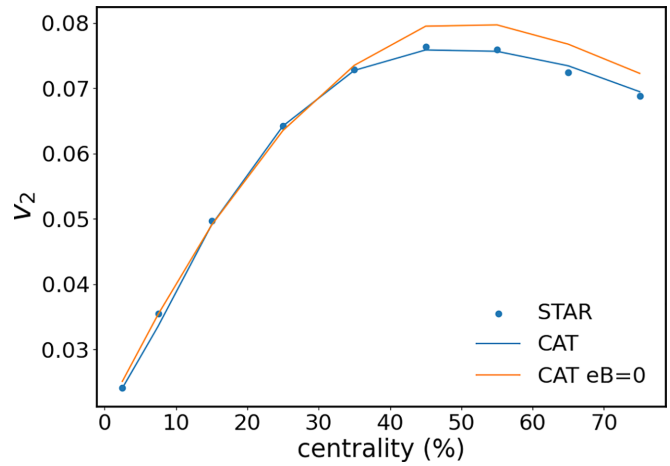


FIG. 2. The CAT result (curve) on the centrality dependence of two-particle $v_2\{2\}$ for charged hadrons in Au+Au collisions at 200 GeV, compared with the STAR data (circles).

Results. The background of the CME is known to be proportional to the ratio of elliptic flow to multiplicity, i.e., $\Delta\gamma \sim -v_2/N$. In order to reproduce the reliable background, we first calculate the elliptic flow $v_2\{2\}$ of charged particles using the two-particle correlation method within the kinetic cut $0.15 < p_T < 2$ GeV/c and $|\eta| < 1$ [48],

As shown in Fig. 2, where our definition of centrality is the same as in experiments by using the reference multiplicity distribution, v_2 is observed to be suppressed in the presence of the magnetic field. On the other hand, the p_T distributions of multiplicity are calculated within the pseudorapidity window of $|\eta| < 0.5$. Figure 3 shows the CAT results on this p_T distribution for different centrality bins, in comparison with the STAR data.

We find that our results can describe the experimental data well. Therefore, we believe that our CAT model provides a reliable description of the CME background. We also check that if we switch off the magnetic field or μ_5, the elliptic flow and the multiplicity distributions are almost unchanged.

The chiral anomaly and the magnetic field can induce a charge current through the chiral magnetic effect. In Fig. 4, we present the results from the CAT simulation with both the magnetic field and the initial net chirality, which show the time evolution of the net-charge density distribution for

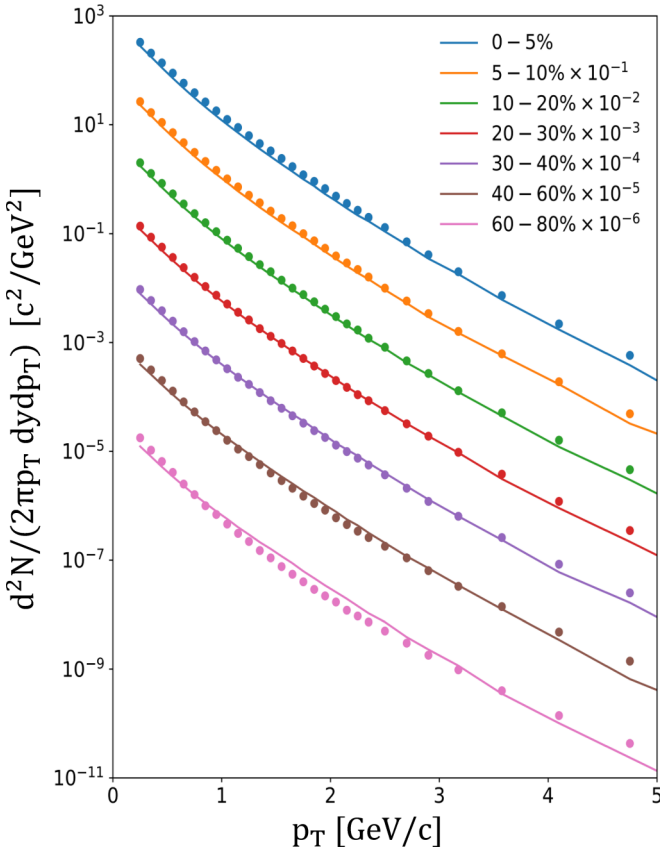


FIG. 3. The CAT results (curves) on p_T distributions of $\frac{1}{2\pi p_T}\frac{d^2N}{dp_T d\eta}$ for multiplicity of charged hadrons of $|\eta| < 0.5$ for different centralities in Au+Au collisions at 200 GeV, compared with the STAR data (circles).

the charged quarks within the range $|\eta| < 1$ in the transverse plane. This simulation demonstrates the generation of the CME-induced charge separation along the direction of the magnetic field due to chiral anomaly transport. Initially, the net-charge density increases and then slowly decreases with the decay of the magnetic field and the expansion of the QGP. We have verified that this charge separation disappears when the chiral magnetic effect cannot occur, which happens when the chiral chemical potential equals zero.

The generation of the chiral magnetic effect contributes to the total two-particle correlation $\gamma_{\rm total}$. On the other hand, the chiral magnetic effect does not occur in the absence of chiral anomaly. Therefore, only the background $\gamma_{\rm bkg}$ can be obtained without the chiral anomaly, which is the total background including the flow background, the nonflow background, and the effect of the Lorentz force. Figure 5 shows the centrality dependencies of the opposite-sign correlation $\gamma_{\rm os}$, the same-sign $\gamma_{\rm ss}$ correlation, and the correlation difference $\Delta\gamma = \gamma_{\rm os} - \gamma_{\rm ss}$ in Au + Au collisions at 200 GeV, compared with the AMPT model result [22,32] and the STAR data [28]. We observe that the CAT model with the chiral anomaly outperforms the other cases in describing the STAR data. In this optimal case, we take

$$\mu_5 = (2.1T + \sqrt{eB})\ \text{GeV}, \tag{8}$$

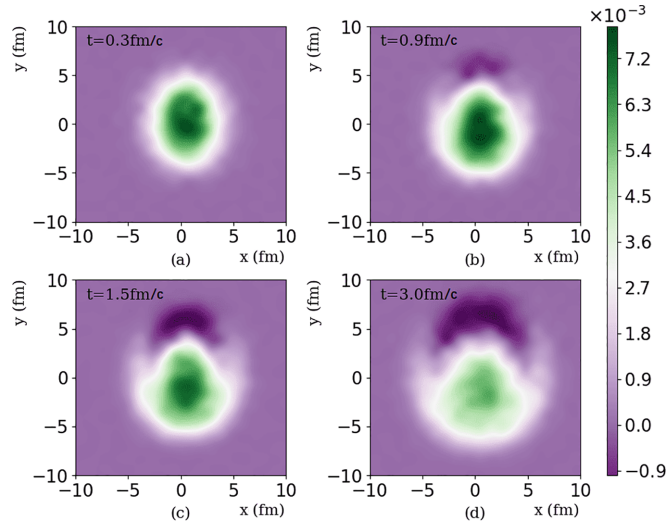


FIG. 4. The CAT results on the distributions of net-charge density in the transverse plane at $t = 0.3$, 0.9, 1.5, and 3.0 fm/c, respectively, during the partonic evolution at $b = 8$ fm and $\mu_5 > 0$.

and its magnitude is consistent with the effective chiral chemical potential induced by axial-vector interactions [49,50]. The chiral anomaly influences both the same-sign and the opposite-sign correlations, with different significance for each centrality. For instance, in the 20–50% centrality, $\gamma_{\rm ss}$ increases with n_5, while $\gamma_{\rm os}$ remains almost unchanged. We notice that the correlations are more sensitive to axial anomaly in the middle centrality 20–50%, but in centrality 60–70%, the difference is negligible within the error. Compared to the previous AMPT study, we observe that the CME leads to nearly zero change of $\gamma_{\rm ss}$ in the 0–50% centrality and rapidly

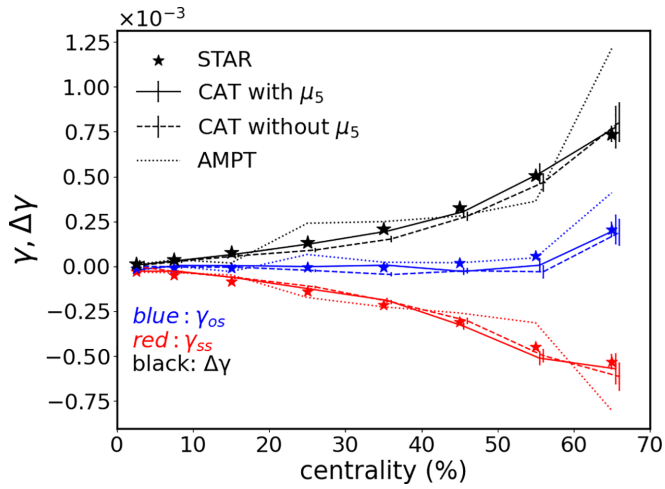


FIG. 5. The CAT results on the centrality dependencies of the correlations of opposite-sign $\gamma_{\rm os}$, same-sign $\gamma_{\rm ss}$, and the difference $\Delta\gamma = \gamma_{\rm os} - \gamma_{\rm ss}$ in Au+Au collisions at 200 GeV, compared with the STAR data (stars) and the AMPT result (dot curves), where the different colors represent different correlations. The CAT results are calculated by the CAT with and without the chiral chemical potential μ_5, shown by solid and dashed curves, respectively.

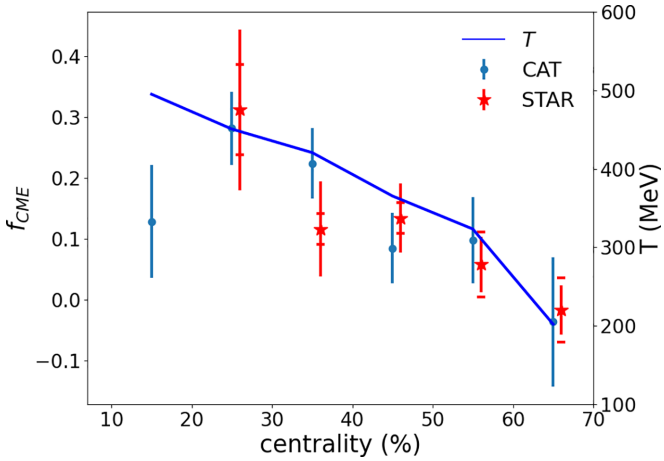


FIG. 6. The CAT result (circles) on the centrality dependence of the CME fraction $f_{\rm CME}$, compared with the STAR data (stars) [27] and the centrality dependence of the average temperature of the fireball (line).

increases $\gamma_{\rm os}$ in 50–70%, more consistent with the STAR data. In general, we observe a difference in the 10–70% centrality with and without the chiral anomaly, indicating the presence of the CME signal.

In order to extract the contribution of the CME signal to the total γ correlation, the CME signal fraction is defined as

$$f_{\rm CME} = \frac{\Delta\gamma_{\rm CME}}{\Delta\gamma_{\rm total}} = \frac{\Delta\gamma_{\rm total} - \Delta\gamma_{\rm bkg}}{\Delta\gamma_{\rm total}}. \tag{9}$$

Figure 6 shows the CAT result on the centrality dependence of the CME fraction $f_{\rm CME}$, compared with the STAR data [27]. The CME fraction decreases from central to peripheral collisions, in good agreement with recent STAR measurement. We observe an increase in the CME signal from central to peripheral collisions, but a decrease in the CME signal fraction, indicating greater background in peripheral collisions. We also notice that the tendency of the CME fraction $f_{\rm CME}$ follows the tendency of centrality dependence of the temperature.

Conclusion. Based on the AMPT model, we develop a new module of CAT to solve the chiral kinetic equation in order to trace the evolution of the initial topological charge under the magnetic field, and we trace the separation of charged particles induced by the CME, thus providing a quantitative connection between the initial topological charge and the eventual experimental signal of the CME in heavy-ion collisions.

For Au+Au collisions at an energy of 200 GeV, the magnetic field is calculated from the HIJING module and the initial chirality imbalance is given as $\mu_5 = (2.1T + \sqrt{eB})$ GeV; then the CAT module solves the evolution of the chiral anomaly with the decay of the magnetic field. The CAT simulation shows the development of the CME-induced charge separation along the direction of the magnetic field due to chiral anomaly transport, and the results of the OS correlator $\gamma_{\rm os}$ and the SS correlator $\gamma_{\rm ss}$, as well as their difference $\Delta\gamma$, are quantitatively consistent with the STAR measurement. The background of CME, $\gamma_{\rm bkg}$, is regarded as in the case without initial chiral anomaly, and the signal of the CME fraction $f_{\rm CME}$ decreases from central to peripheral collisions, which is in good agreement with recent STAR measurements. It is observed that the OS and SS correlators of the CME signal increase from central to peripheral, but the signal of the CME fraction decreases from central to peripheral, and the tendency of the CME fraction $f_{\rm CME}$ follows the tendency of centrality dependence of the fireball temperature.

For a next step, we will investigate the evolution of chiral anomaly in isobar collisions and Au+Au collisions at low energies.

Acknowledgments. This work is supported in part by the National Natural Science Foundation of China (NSFC) under Grants No: 12235016, No. 12325507, No. 12221005, No. 12147150, No. 12375121, No. 12205309, No. 12147101, No. 12347143, and No. 12347106; the Strategic Priority Research Program of Chinese Academy of Sciences under Grant No XDB34030000; the Fundamental Research Funds for the Central Universities; and the Natural Science Basic Research Program of Shaanxi (Program No. 2023-JC-QN-0267).

[1] V. A. Kuzmin, V. A. Rubakov, and M. E. Shaposhnikov, On the anomalous electroweak baryon number nonconservation in the early universe, Phys. Lett. B **155**, 36 (1985).
[2] M. E. Shaposhnikov, Baryon asymmetry of the universe in standard electroweak theory, Nucl. Phys. B **287**, 757 (1987).
[3] V. A. Rubakov and M. E. Shaposhnikov, Electroweak baryon number nonconservation in the early universe and in high-energy collisions, Usp. Fiz. Nauk **166**, 493 (1996).
[4] A. A. Belavin, Alexander M. Polyakov, A. S. Schwartz, and Yu. S. Tyupkin, Pseudoparticle solutions of the Yang-Mills equations, Phys. Lett. B **59**, 85 (1975).
[5] E. Witten, Current algebra theorems for the U(1) Goldstone boson, Nucl. Phys. B **156**, 269 (1979).
[6] G. Veneziano, U(1) without instantons, Nucl. Phys. B **159**, 213 (1979).
[7] E. Vicari and H. Panagopoulos, Theta dependence of SU(N) gauge theories in the presence of a topological term, Phys. Rep. **470**, 93 (2009).
[8] T. Schäfer and E. V. Shuryak, Instantons in QCD, Rev. Mod. Phys. **70**, 323 (1998).
[9] D. Kharzeev, R. D. Pisarski, and M. H. G. Tytgat, Possibility of spontaneous parity violation in hot QCD, Phys. Rev. Lett. **81**, 512 (1998).
[10] D. Kharzeev and R. D. Pisarski, Pionic measures of parity and CP violation in high-energy nuclear collisions, Phys. Rev. D **61**, 111901(R) (2000).
[11] D. Kharzeev, A. Krasnitz, and R. Venugopalan, Anomalous chirality fluctuations in the initial stage of heavy ion collisions and parity odd bubbles, Phys. Lett. B **545**, 298 (2002).
[12] D. Kharzeev, Parity violation in hot QCD: Why it can happen, and how to look for it, Phys. Lett. B **633**, 260 (2006).
[13] K. Fukushima, D. E. Kharzeev, and H. J. Warringa, The chiral magnetic effect, Phys. Rev. D **78**, 074033 (2008).
[14] D. E. Kharzeev, J. Liao, S. A. Voloshin, and G. Wang, Chiral magnetic and vortical effects in high-energy nuclear collisions—A status report, Prog. Part. Nucl. Phys. **88**, 1 (2016).

[15] M. Abdallah *et al.*, Search for the chiral magnetic effect with isobar collisions at $\sqrt{s_{NN}} = 200$ GeV by the STAR Collaboration at the BNL Relativistic Heavy Ion Collider, Phys. Rev. C **105**, 014901 (2022).

[16] L. Adamczyk *et al.*, Beam-energy dependence of charge separation along the magnetic field in Au+Au collisions at RHIC, Phys. Rev. Lett. **113**, 052302 (2014).

[17] B. Abelev *et al.*, Charge separation relative to the reaction plane in Pb-Pb collisions at $\sqrt{s_{NN}} = 2.76$ TeV, Phys. Rev. Lett. **110**, 012301 (2013).

[18] A. Bzdak, V. Koch, and J. Liao, Remarks on possible local parity violation in heavy ion collisions, Phys. Rev. C **81**, 031901(R) (2010).

[19] F. Wang, Effects of cluster particle correlations on local parity violation observables, Phys. Rev. C **81**, 064902 (2010).

[20] S. Schlichting and S. Pratt, Charge conservation at energies available at the BNL Relativistic Heavy Ion Collider and contributions to local parity violation observables, Phys. Rev. C **83**, 014913 (2011).

[21] W.-Y. Wu *et al.*, Global constraint on the magnitude of anomalous chiral effects in heavy-ion collisions, Phys. Rev. C **107**, L031902 (2023).

[22] G.-L. Ma and B. Zhang, Effects of final state interactions on charge separation in relativistic heavy ion collisions, Phys. Lett. B **700**, 39 (2011).

[23] J. Zhao and F. Wang, Experimental searches for the chiral magnetic effect in heavy-ion collisions, Prog. Part. Nucl. Phys. **107**, 200 (2019).

[24] F.-Q. Wang and J. Zhao, Search for the chiral magnetic effect in heavy ion collisions, Nucl. Sci. Tech. **29**, 179 (2018).

[25] H.-J. Xu, J. Zhao, X. Wang, H. Li, Z.-W. Lin, C. Shen, and F. Wang, Varying the chiral magnetic effect relative to flow in a single nucleus-nucleus collision, Chin. Phys. C **42**, 084103 (2018).

[26] B.-X. Chen, X.-L. Zhao, and G.-L. Ma, Difference between signal and background of the chiral magnetic effect relative to spectator and participant planes in isobar collisions at $\sqrt{s_{\rm NN}} =$ 200 GeV. Phys. Rev. C **109**, 024909 (2024).

[27] M. S. Abdallah *et al.*, Search for the chiral magnetic effect via charge-dependent azimuthal correlations relative to spectator and participant planes in Au + Au collisions at $\sqrt{s_{NN}} = 200$ GeV, Phys. Rev. Lett. **128**, 092301 (2022).

[28] B. I. Abelev *et al.*, Observation of charge-dependent azimuthal correlations and possible local strong parity violation in heavy ion collisions, Phys. Rev. C **81**, 054908 (2010).

[29] D. E. Kharzeev, J. Liao, and S. Shi, Implications of the isobar-run results for the chiral magnetic effect in heavy-ion collisions, Phys. Rev. C **106**, L051903 (2022).

[30] S. Shi, Y. Jiang, E. Lilleskov, and J. Liao, Anomalous chiral transport in heavy ion collisions from anomalous-viscous fluid dynamics, Ann. Phys. **394**, 50 (2018).

[31] A. Huang, S. Shi, S. Lin, X. Guo, and J. Liao, Accessing topological fluctuations of gauge fields with the chiral magnetic effect, Phys. Rev. D **107**, 034012 (2023).

[32] W.-T. Deng, X.-G. Huang, G.-L. Ma, and G. Wang, Predictions for isobaric collisions at $\sqrt{s_{\rm NN}} = 200$ GeV from a multiphase transport model, Phys. Rev. C **97**, 044901 (2018).

[33] X.-L. Zhao and G.-L. Ma, Search for the chiral magnetic effect in collisions between two isobars with deformed and neutron-rich nuclear structures, Phys. Rev. C **106**, 034909 (2022).

[34] V. Koch, S. Schlichting, V. Skokov, P. Sorensen, J. Thomas, S. Voloshin, G. Wang, and H.-U. Yee, Status of the chiral magnetic effect and collisions of isobars, Chin. Phys. C **41**, 072001 (2017).

[35] Z.-W. Lin, C. M. Ko, B.-A. Li, B. Zhang, and S. Pal, A Multi-phase transport model for relativistic heavy ion collisions, Phys. Rev. C **72**, 064901 (2005).

[36] D. T. Son and N. Yamamoto, Berry curvature, triangle anomalies, and the chiral magnetic effect in Fermi liquids, Phys. Rev. Lett. **109**, 181602 (2012).

[37] M. A. Stephanov and Y. Yin, Chiral kinetic theory, Phys. Rev. Lett. **109**, 162001 (2012).

[38] A. Huang, S. Shi, Y. Jiang, J. Liao, and P. Zhuang, Complete and consistent chiral transport from Wigner function formalism, Phys. Rev. D **98**, 036010 (2018).

[39] W.-H. Zhou and J. Xu, Simulating the chiral magnetic wave in a box system, Phys. Rev. C **98**, 044904 (2018).

[40] Y. Sun and C. M. Ko, Chiral kinetic approach to the chiral magnetic effect in isobaric collisions, Phys. Rev. C **98**, 014911 (2018).

[41] J.-W. Chen, Jin-yi Pang, S. Pu, and Q. Wang, Kinetic equations for massive Dirac fermions in electromagnetic field with non-Abelian Berry phase, Phys. Rev. D **89**, 094003 (2014).

[42] Y. Chen, X.-L. Sheng, and G.-L. Ma, Electromagnetic fields from the extended Kharzeev-McLerran-Warringa model in relativistic heavy-ion collisions, Nucl. Phys. A **1011**, 122199 (2021).

[43] L. McLerran and V. Skokov, Comments about the electromagnetic field in heavy-ion collisions, Nucl. Phys. A **929**, 184 (2014).

[44] W.-T. Deng and X.-G. Huang, Event-by-event generation of electromagnetic fields in heavy-ion collisions, Phys. Rev. C **85**, 044907 (2012).

[45] Z.-W. Lin, Evolution of transverse flow and effective temperatures in the parton phase from a multi-phase transport model, Phys. Rev. C **90**, 014904 (2014).

[46] J. Chao, P. Chu, and M. Huang, Inverse magnetic catalysis induced by sphalerons, Phys. Rev. D **88**, 054009 (2013).

[47] G. Başar and D. E. Kharzeev, The Chern-Simons diffusion rate in strongly coupled $N = 4$ SYM plasma in an external magnetic field, Phys. Rev. D **85**, 086012 (2012).

[48] N. Borghini, P. M. Dinh, and J.-Y. Ollitrault, Flow analysis from multiparticle azimuthal correlations, Phys. Rev. C **64**, 054901 (2001).

[49] L. Yu, H. Liu, and M. Huang, Spontaneous generation of local CP violation and inverse magnetic catalysis, Phys. Rev. D **90**, 074009 (2014).

[50] J. Shao and M. Huang, Gravitational waves and primordial black holes from chirality imbalanced QCD first-order phase transition with $\mathcal{P}$ and $\mathcal{CP}$ violation, Phys. Rev. D **107**, 043011 (2023).